DOI: 10.13009/EUCASS2019-92

Investigation on the supplementary combustion scheme for the divergent section of a solid rocket engine nozzle

Zhao-bo Du

College of Aerospace Science and Engineering, National University of Defense Technology, Changsha, Hunan 410073, China. e-mail: 13159861797@163.com

Wei Huang

College of Aerospace Science and Engineering, National University of Defense Technology, Changsha, Hunan 410073, China. e-mail: gladrain2001@163.com

Li Yan

College of Aerospace Science and Engineering, National University of Defense Technology, Changsha, Hunan 410073, China. e-mail: scarlet@163.com

Abstract

The low combustion efficiency of the propellant results in the small specific impulse of the solid rocket engine. This paper attempts to install the inlet on the divergent section of the engine nozzle for additional combustion in order to improve the specific impulse of the solid rocket engine. In this paper, the external section, the throat and the divergent section of the inlet are designed by theoretical calculation, programming calculation and numerical simu-lation, and the inlet is installed on the nozzle to carry out the integrated numerical simulation. The obtained results show that there is a high temperature region where the temperature rises sharply upstream of the inlet. Severe com-bustion area which is strip-shaped distribution appears downstream of the air entrance, along the axis direction, parallel to the nozzle wall. Without considering the resistance, the supplementary combustion for the divergent sec-tion of the solid rocket engine nozzle can effectively improve the specific impulse by about 20%.

1. Introduction

The solid rocket engine has a simple structure and superior performance, and it has left an indelible mark in the history of human aerospace [1]. However, due to the lean oxygen characteristics of the propellant, it burns incompletely, and its specific impulse is small accordingly. The small specific impulse is one of the most important key factors to limit its development. Therefore, improving the combustion efficiency of propellants is an important approach to increase the specific impulse. At present, with the solid rocket engine as a prototype, the use of air to supplement the combustion method to improve the specific impulse of the engine is divided into two categories, namely, solid rocket ramjet engine and solid fuel ramjet engine [2]. Both of them have the common aircraft inlet, but also the presence of propellants, which are a new type of propulsion system. The promotion of the specific impulse is very obvious.

Therefore, this article considers a new way to combine the air inlet with the nozzle of the solid rocket engine, and introduce air into the divergent section of the nozzle to supplement the combustion to improve the combustion efficiency of the propellant so as to improve the specific impulse [3].

As for the design of supersonic air inlet, as early as in 1940s and 1950s, the United States carried out a great deal of basic researches in inlet when studying ramjet engines used in air-launched weapons. In the 1980s, NASA extensively studied the aerodynamic characteristics of various configurations of air breathing missiles [4]. In recent years, most countries have designed advanced air-to-air missiles using a binary mixed-compression supersonic inlet and have adopted an integrated design of the missile and air inlet. This represents the research direction in this area. Relevant domestic work started relatively late, but the progress made in recent years is very fast and a lot of fruitful research achievements have also been made. Eagle series of supersonic anti-ship missiles, Perak series of air-to-air missiles have a very high penetration rate and hit rate, which is not unrelated to the excellent design of the inlet. In theoretical research, Wang Q F pointed out the key issues in the design of ramjet missile inlet, including the type, number and location of air inlets, the boundary layers, the compression and shock system, etc., calculate the indispensability of wind tunnel test; Lu X F and Fan S Q calculated and analyzed the influence of flight conditions, ge-

DOI: 10.13009/EUCASS2019-92

ometry and other factors on the main performance parameters of the inlet by numerical simulation of the flow field of the binary mixed-compression supersonic inlet, studied the hypersurface fitting method, obtained a binary mixed-compression supersonic inlet mathematical model [5].

2. Integrated design

In this paper, the design is to install the inlet on the divergent section of the engine nozzle. In order to reduce unnecessary total pressure loss and prevent the outlet pressure of the inlet from being too low, the position behind the engine should be selected when installing. Open the slit in the nozzle divergent segment, according to the pressure at the inlet outlet to choose its connection with the nozzle, according to the literature to determine the interface with the horizontal angle of 30 °. Finally complete the integrated program design. The design result is shown in Fig. 1 [6].

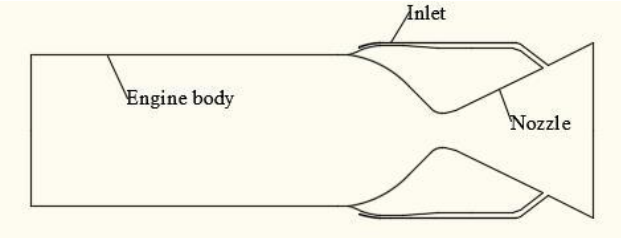

Figure 1: Schematic of the solid rocket engine

3. Inlet design

Taking into the relevant requirements of the inlet design, the starting of the internal compression inlet is difficult. To the external compression inlet, the resistance and the total pressure loss are large. The characteristics of the inlet used in this paper are specific. The type of inlet is chosen as a constant geometry mixed compression inlet, and it has the advantages of light weight, simple structure, high reliability and easy integration design [7][8].
The design height is 10km, the design Mach number is 3.0, the starting Mach number is 2.8 and the design flow is 3.0kg/s.

3.1. Determine the capture area

According to the equations (1) and (2), the static pressure is 26436.2Pa, the temperature is 223.15K, the density is 0.4127kg/m^2, and the capture area is calculated as $A_0 = A_1 = 8267.9\text{mm}^2$.

$$\Phi = \frac{\dot{m}_0}{\dot{m}_1} = \frac{A_0}{A_1} \tag{1}$$

$$m_0 = \rho_\infty v_\infty A_0 \tag{2}$$

3.2. Shock wave system configuration

After determining the configuration of the inlet, and then the inlet shock wave system is obtained. The basic principle is to ensure that the total pressure recovery coefficient as large as possible under the premise of making the number of the equal-strength shock wave as small as possible to ensure that the inlet structure is simple.
The derivation shows that the extreme conditions for obtaining the maximum total pressure recovery coefficient are that the intensities of the oblique shock waves are equal, namely, the normal Mach numbers of the pre-shock are equal.

$$M_1 \sin\beta_1 = M_2 \sin\beta_2 = \cdots = M_{N-1} \sin\beta_{N-1} \tag{3}$$

Herein, β is the shock wave angle.
The static pressure relationship of post-shock and pre-shock is

DOI: 10.13009/EUCASS2019-92

$$\frac{p_{i+1}}{p_i} = \frac{2k}{k+1} M_i^2 \sin^2 \beta_i - \frac{k-1}{k+1} \tag{4}$$

The total pressure relationship of post-shock and pre-shock is

$$\frac{p_{i+1}^*}{p_i^*} = \left[\frac{(k+1) M_i^2 \sin^2 \beta_i}{2 + (k-1) M_i^2 \sin^2 \beta_i}\right]^{\frac{k}{k-1}} \Bigg/ \left[\frac{2k}{k+1} M_i^2 \sin^2 \beta_i - \frac{k-1}{k+1}\right]^{\frac{1}{k-1}} \tag{5}$$

The Mach number relationship of post-shock and pre-shock is

$$M_{i+1}^2 = \frac{M_i^2 + \frac{2}{k-1}}{\frac{2k}{k-1} M_i^2 \sin^2 \beta_i - 1} + \frac{M_i^2 \cos^2 \beta_i}{\frac{k-1}{2} M_i^2 \sin^2 \beta_i + 1} \tag{6}$$

In the equations (4) to (6), p_i means the pre-shock static pressure, p_{i+1} is the post-shock static pressure, M_i means the pre-shock Mach number, M_{i+1} is the post-shock Mach number, p_i^* means the pre-shock total pressure, and p_{i+1}^* is the post-shock total pressure.

In principle, the setting of the wedge angle is based on the maximum total pressure recovery coefficient, according to the best wave theory [9]. The C + + language is used to write programs, with single wedge angle as example and the block diagram is shown in Fig. 2. Under the designed point, there are two oblique shock waves and one positive shock wave. The wedge angles are 14.99 °and 18.82 °respectively, and the optimal solution of total pressure recovery coefficient is 0.744.

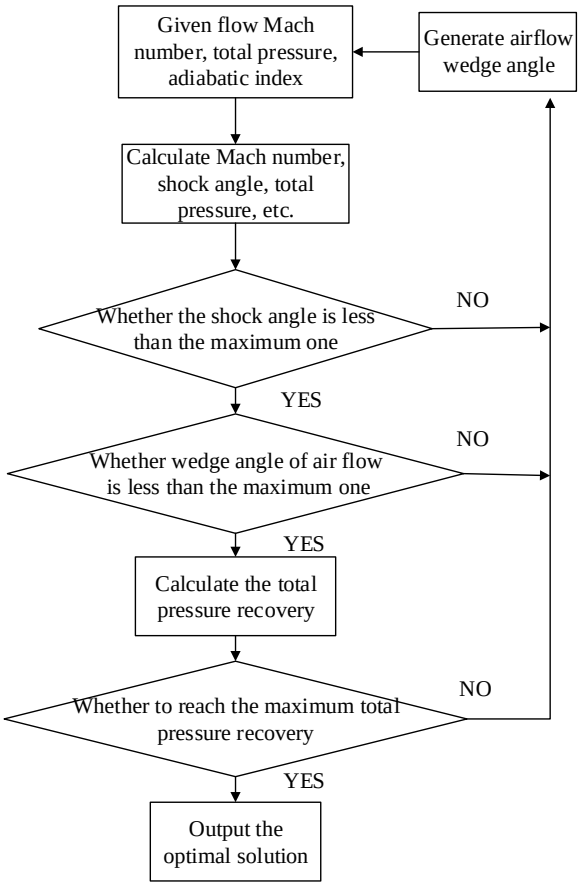

Fig.2: Schematic of the program

DOI: 10.13009/EUCASS2019-92

3.3. The choice of lip angle of the cowl and compression surface position

The design of the lip of the cowl should be based on the principle that the shock waves will intersect on the lip, and at the same time make the resistance of the cowl as small as possible. The angle of the lip of the cowl is generally around 2 °~ 4 °. In this paper, it is selected as 3 °.
With respect to the location of the compression surface relative to the lip, this paper considers the length of the compression surface, the small mass of the structure, the small additional resistance, the design of the internal passageway. The way chooses that shock waves intersect. Finally, the front edge of the lip of the cowl is with a small blunt body rather than a complete sharp.

3.4. Throat design

In order to meet the requirement of self-starting, the throat area should be larger than the minimum throat area required for starting [10]. The minimum throat area required for self-starting inlet is given by Eq. (7).

$$A_t = \frac{\phi_{\max} q(\lambda_\infty)}{0.98\sigma_a} A_1 \tag{7}$$

Herein, A_t is the inlet throat area, $\Phi_{\max}$ is the maximum flow coefficient, which is 1 when in design state, $q(\lambda_\infty)$ is the aerodynamic function of the incoming flow at a given flight Mach number, σ_a is the total pressure recovery coeffi-cient before throat post positive shock, and A_1 is the cross-sectional area of the inlet. In this paper, the calculation of the inlet throat area is 2026.91mm^2.
The height of the throat depends on the starting requirements of the inlet. According to the calculation, the throat height is 5.0 mm. For the length of the isolation section, the numerical simulation shows that the isolation section too long or too short will shock off the inlet. With the flow Mach number changes, isolation section length to height ratio will change, and in line with law. This design of the isolation section length is 40.07mm.

3.5. Design of subsonic velocity divergent section

Under normal circumstances, in order to prevent the separation of the flow in subsonic velocity divergent segment, we should mainly control the two parameters, one is that the Mach number post the last positive shock wave does not exceed 0.8, the second is the maximum wedge angle not more than 8 °[11]. This article is the choice of equal wedge angle design. According to requirements, the angle of the paper is chosen for 5 °. With respect to the length of the divergent section, a numerical simulation of the length of various divergent sections is performed in this paper, keeping the other inlet parameters unchanged. The results show that too long or too short divergent section will make the shock wave off the inlet. According to the simulation results, the length of the divergent section is selected to be 74.39mm.

3.6. The results of inlet design

According to the requirements of the integrated design parameters, the theory to calculate, while optimizing the wedge angle and total pressure recovery coefficient programming, numerical simulation to determine the length of the isolation section and the divergent section [12][13], we ultimately get a more ideal inlet model, as shown in Fig. 3 and Table.1.

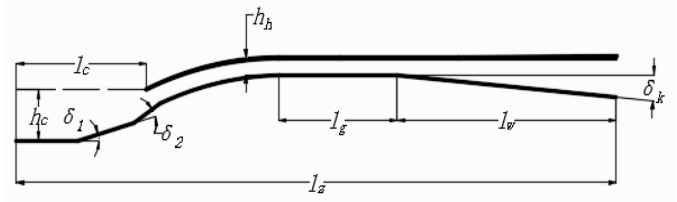

Fig.3: Schematic of the intake.

Table.1: Geometric dimensions of the intake.

Parameters	Values

DOI: 10.13009/EUCASS2019-92

The first level of wedge angle δ_1	14.99 °
The second level of wedge angle δ_2	18.82 °
Angle of the lip of the cowl	3 °
Horizontal length of lip l_c /mm	44.18
Height of lip/mm	14.97
Height of throat h_h /mm	5
Length of isolation section l_g /mm	40.07
Wedge angle of divergent section δ_k	5 °
Length of divergent section l_w /mm	74.39
Length of inlet l_z /mm	203.01

4. Results and discussion

4.1. Code validation

Reinartz et al. [14][15] conducted a large number of numerical simulations and ground experimental tests on a two-dimensional supersonic inlet, and they obtained good results. In this section, one of the models tested by Reinartz et al. [15] is employed, see Fig.4, and the correctness of the numerical approaches used for the supersonic inlet is verified based on the experimental schlieren map, see Fig.5. The length of the isolator (l) is chosen to be 79.3 mm [16][17].

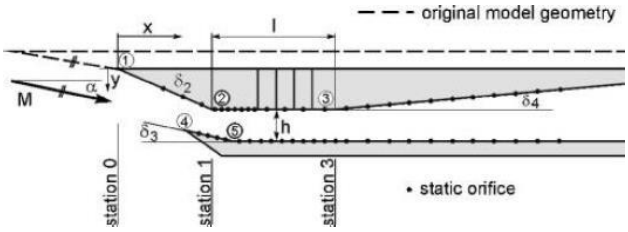

Fig. 4: Geometric configuration of the supersonic inlet.

The inlet flow conditions are set as follows. The freestream Mach number is that Ma_∞= 2.41, the static pressure is 319kPa and the flow angle of attack is 10° . The Standard κ - ε model [18] is selected to be the turbulence model, and the second-order spatially accurate upwind scheme that applies the advection upstream splitting method (AUSM) for the flux vector is utilized. The Green-Gauss cell-based gradient method is employed to compute the gradients, and the Courant-Friedrichs-Levy number is maintained at 0.5 by using proper under-relaxation factors to ensure stability [19][20].

At the same time, the grid independence analysis is carried out, and three different grid scales are taken into consideration, namely the coarse grid, the moderate grid and the refined grid. The structured grid is used to calculate the inlet flow field, and the grids are clustered at the corner of the walls and near the walls [21]. The number of the grid cells for the coarse grid, the moderate grid and the refined grid is 32733, 125507 and 487221 respectively.

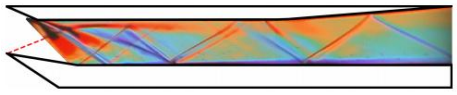

Fig.5: Experimental schlieren map.

Fig.6: Density gradient diagram obtained by the coarse grid.

DOI: 10.13009/EUCASS2019-92

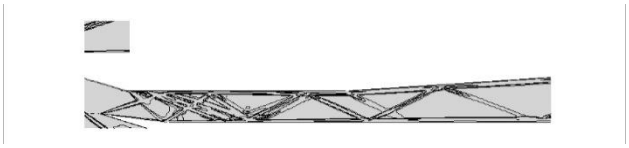

Fig.7: Density gradient diagram obtained by the moderate grid.

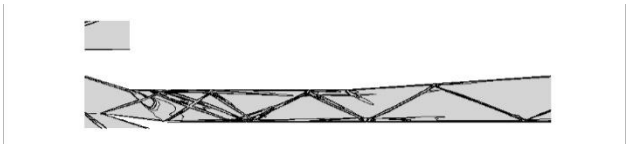

Fig.8: Density gradient diagram obtained by the refined grid.

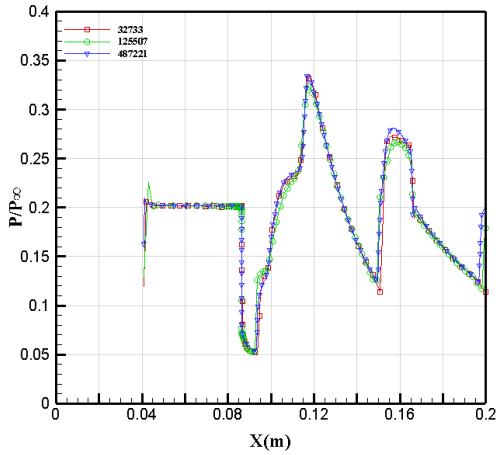

Fig.9 Comparison of the pressure ratio distributions along the ramp obtained by three different grid scales.

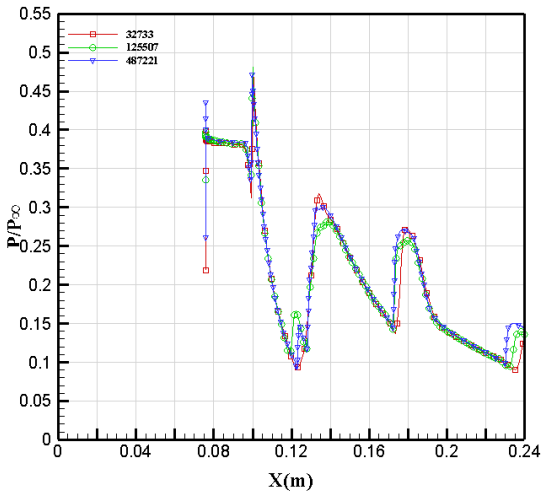

Fig.10 Comparison of the pressure ratio distributions along the cowl obtained by three different grid scales.

It can be seen from Figs.5-8, the flow field structures in the inlet obtained by three different grid scales show good agreement with the experimental schlieren map. At the same time, it is obvious that the grid scale has only slight difference on the pressure ratio distributions along the ramp and cowl, see Figs.9 and 10. This implies that the numerical approaches, as well as the grid scale, are with confidence to carry out the following investigations.

4.2. Inlet numerical simulation

In order to evaluate the performance of the inlet, the flow field structures in the inlet are obtained by the numeri-cal simulation, and the grids of the boundary layer are established specially in order to simulate the gas flow near the wall and to reflect the shock wave structure variations better. Finally, the total number of grid cells is 50784, and Fig.11 shows the grid system employed in the inlet.

The pressure diagram and Mach number diagram are shown as Fig. 12 and Fig. 13. From Fig. 12 and Fig. 13, the incoming stream of supersonic air flow encountered in the process of obstruction, resulting in shock wave. In this process, the total enthalpy is constant, the total pressure suddenly drops, the static temperature, static pressure and density decrease, the entropy value suddenly increases, and the speed finally decreases. Meanwhile, as can be seen

DOI: 10.13009/EUCASS2019-92

from Fig. 12 and Fig. 13, the compressional wave system of the external section, the expansion wave system of the lip section and the shock wave chain in the divergent section are calculated. Under the design Mach number, there are three main shock waves in the external section of the inlet. The first two oblique shock waves intersect on the lip of the cowl, and the performance of the inlet does not deteriorate. After three shocks, the airflow is compressed by the supersonic speed into subsonic speed, and then enters the isolator, continues to decelerate and pressurize, and finally reaches the outlet of the inlet uniformly and stably.
Based on the numerical results, the total pressure of export of the inlet is 655398.56Pa, the average static pressure is 40597.23Pa, the total pressure ratio is 0.675, the flow rate is 3.44kg/s and the total pressure ratio is 0.744 in theory. The total pressure ratio and flow rate are compared with the design values, which is still within the scope of the de-sign requirements of this article, so the inlet design results are good.

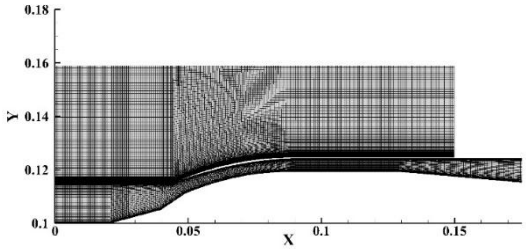

Fig.11 Mesh division results of the inlet.

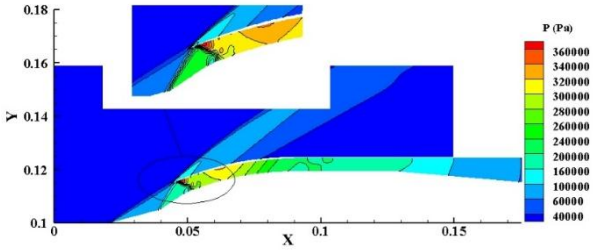

Fig.12 Pressure contour under design condition.

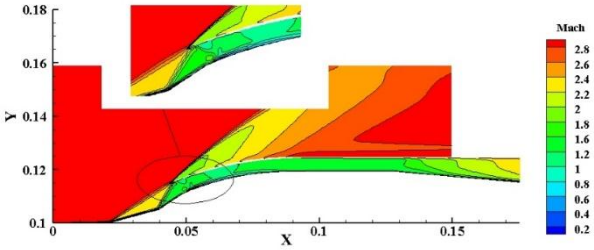

Fig.13 Mach number contour under design condition.

4.3. Nozzle selection

In order to test the effect of increasing the specific impulse of the engine on the inlet, an engine is selected, which is mainly the nozzle section [22]. The working pressure of the engine is 7.0Mpa, the total impulse is 120kN s, the thrust is 50kN, the propellant is CTPB/AP/Al, the metal content is 16.0%, the theoretical specific impulse is 260s and the diameter is 200mm.
Through calculation, the designed flow is = 19.6kg/s, nozzle throat diameter is 72mm, and nozzle outlet di-ameter is 360mm. The structure diagram is shown in Fig.14. At the same time, the numerical simulation of the noz-zle is taken. The simulation results and theoretical calculations are compared, as shown in Table.2. The comparison shows that the design result is good.

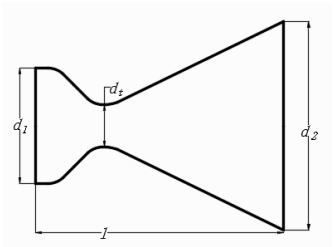

Fig.14 Schematic diagram of the nozzle.

Table.2 Comparison of the design results of the nozzle.

Parameters	Theoretical calculation	Numerical simulation
Flow/kg/s	19.60	19.62
Total thrust/kN	50.00	44.85

DOI: 10.13009/EUCASS2019-92

Total impulse/kN s	120.00	107.66
Specific impulse/s	260.00	223.26
Pressure ratio	0.0038	0.0022

4.4. The integrated program numerical simulation

When simulating the integrated design scheme, the type of solver is selected as two-dimensional single-precision density-based solver, and the coupled implicit solution method and steady-state calculation are selected. The governing equations are selected as the axisymmetric Reynolds averaged N-S equations [23][24].
When starting the calculation, use a non-stick model and wait until the flow field is stable. Select the standard κ-ε turbulence model [25] and add the chemical reaction until the result converges [26]. Among them, at the entrance of the inlet, the mole fraction of N_2 and O_2 in air is 79% and 21% respectively. In the nozzle divergent section, the gas consists of CO, H_2, SO_2, N_2, H_2O and other gases (the same as when no additional combustion is carried out). Calculated by the chemical equilibrium constant method, the obtained results are shown in Table .3.

Table.3 Gas mole component in the divergent section of the nozzle.

	CO	H_2	SO_2	N_2	H_2O	Other
Mole fraction/%	26.26	28.43	6.05	7.24	15.39	16.63

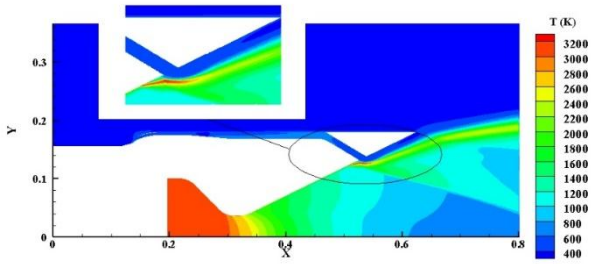

Fig.15 Temperature profile.

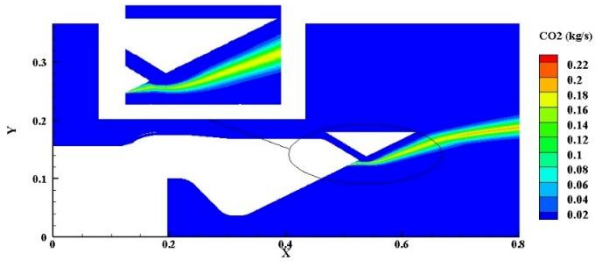

Fig.16 CO_2 profile.

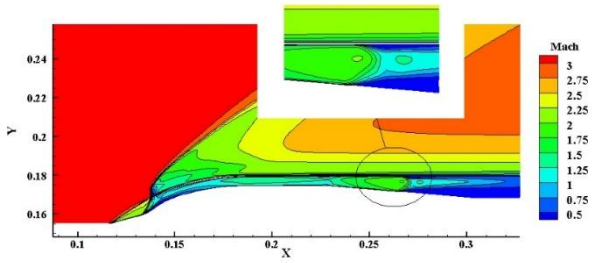

Fig.17 Mach number contour at the air intake.

DOI: 10.13009/EUCASS2019-92

Table.4 Comparison of nozzle and integrated simulation results.

Parameters	Nozzle	Integration	Growth rate/%
Gas flow/kg/s	19.62	18.21	——
Air flow/kg/s	——	4.70	——
Total thrust/kN	44.85	47.73	6.42
Total impulse/kN s	107.66	130.61	21.32
Specific impulse/s	223.26	282.99	26.75

The temperature, density, Mach number and CO_2 distribution in gas components are shown in figures. Analysis of the recycle flow field is as follows:

(1) From Fig. 15, a high temperature region where the temperature rapidly rises appears upstream of the air inlet. From the analysis, it can be seen that the air is decelerated and pressurized into the nozzle through the inlet, and the flammable components of incomplete combustion in the nozzle and the O_2 in the air are burned completely, resulting in a sharp increase in temperature. Downstream of the air inlet, the temperature is much reduced, which effectively reduces the gas ablation to the nozzle.

(2) From Fig. 16, it can be seen clearly that the area supplemented by severe combustion is located downstream of the entrance and along the axial direction, substantially parallel to the wall of the nozzle. The area is strip-shaped and deflected slightly according to the main air flow. There is almost no CO present in the inlet flow, so CO_2 is only generated from the CO reheating caused by incomplete combustion in the nozzle. Therefore, the distribution of CO_2 can accurately reflect the area where the reheating occurs violently.

(3) From Fig. 17, after integration calculation, an overflow occurs at the entrance of the air inlet. A positive shock wave exists in the divergent section of the inlet. An arcuate shock wave is generated at the air entrance and an expansion wave is generated. As the pressure in the inlet divergent section increases, the incoming air cannot enter the nozzle smoothly, while the nozzle expands to produce a plug. And the air continues to be replenished, creating a violent collision and forming a positive shock wave. Overflow occurs at the entrance of the air inlet and the total pressure recovery factor decreases from 0.675 to 0.355. In the divergent section of the nozzle, the air flow converges into the gas flowing at high speed. Due to the difference of velocity and pressure, it follows the flowing tendency of the main body of air flow and forms an arcuate shock wave.

(4) Through numerical simulation, a series of parameters such as engine thrust and gas flow rate are obtained, as shown in Table.4. The CO combustion amount is 0.21 kg/s, the combustion amount of H_2 is 0.01 kg/s, and the air-fuel ratio is 27.31%. As can be seen from Table.4, after the nozzle is equipped with the intake air to make up the combustion, the total thrust is increased by 6.42%, the total impulse is increased by 21.32% and the specific impulse is increased by 26.75%.

5. Conclusions

(1) For the inlet design, at the design Mach number, the oblique shock of the external section of the inlet intersects on the lip of the cowl. There is a shock seal at the lip, and no overflow occurs. Post shocks the flows are compressed, the supersonic velocity changes to subsonic, and then it enters the isolation section and the divergent section. The airflow continues to decelerate and pressurize, and finally the airflow reaches the outlet uniformly and stably.

(2) For the integrated design simulation results, a high temperature region with a sharp increase in temperature appears upstream of the air inlet. Supplementary combustion of the intense area is downstream of the entrance, along the axis direction, substantially parallel to the wall of the nozzle. An overflow occurs at the entrance of the inlet, and a positive shock exists in the divergent of the inlet. An arcuate shock exists at the air inlet, and an expan-sion wave is generated.

(3) After installing the nozzle into the air inlet, the calculation ignores the air resistance and friction resistance. In the end, the total thrust is increased by 6.42%, the total impulse is increased by 21.32% and the specific impulse is increased by 26.75%. This design shows that the way to add the inlet to the rocket engine using the oxygen poor propellant can effectively increase the specific impulse.

DOI: 10.13009/EUCASS2019-92

References

[1]. Li Y M, et al. Solid rocket engine principle. Beijing: Beijing University of Aeronautics and Astronautics Press, 1991: 6-12.
[2]. Bao F T, et al. Solid rocket stamping combined engine. Beijing: China Aerospace Press, 2006:1-25.
[3]. Dhinagaran R, Bose T K. Comparison of Euler and Naiver-Stokes solutions for nozzle flows with secondary injection. AIAA 1996-0453, 1996.
[4]. Dong J F. Design and experimental study of two element mixed pressure supersonic inlet. Xi'an: Northwestern Polytechnical University, 2007.
[5]. Lu X F. Study on flow field calculation and mathematical model of supersonic inlet port. Xi'an: Northwestern Polytechnical University, 2003.
[6]. Wing D J, Giuliano V J. Fluidic thrust vectoring of an axisymmetric exhaust nozzle at static conditions. FEDSM 97-3228
[7]. Xie L R, Guo L R. Numerical simulation and experimental verification of the aerodynamic characteristics of certainly symmetric symmetrical supersonic inlet. Journal of Aeronautics, 2007, 28(1): 78-83.
[8]. Mo Z, Wang X Y. Numerical simulation of slotted axial symmetrical inlets. Computer Simulation, 2008, 25(12): 95-97.
[9]. Zhu Y, Li T, Li C. CFD status for supersonic inlet design support. Aircraft Design, 2002(10):19-21.
[10]. Carrier G, Knight D, Rasheed K, Montazel X. Multi-criteria design optimization of two-dimensional supersonic inlet. AIAA Paper 2001-1064, 2001
[11]. Baddeley A, Logie R, Nimmo-Smith I. Components of fluent reading. Journal of Memory & Language, 1985, 24(1):119-131.
[12]. Van Wie D M. Scramjet inlet, Scramjet propulsion. AIAA 2000, 189(447-511).
[13]. Huang W, Wang Z G, Pourkashanian M, Ma L, Ingham D B, Luo S B, Lei J, Liu J. Numerical investigation on the shock wave transition in a three-dimensional scramjet isolator. Acta Astronautica, 2011, 68, 1669-1675.
[14]. Herrmann C D and Koschel W W. Experimental investigation of the internal compression of a hypersonic intake. AIAA Paper 2002-4130, 2002.
[15]. Reinartz B U, Herrmann C D and Ballmann J. Aerodynamic performance analysis of a hypersonic inlet isolator using computation and experiment. Journal of Propulsion and Power, 2003, 19(5): 868-875.
[16]. Schmitz M C and Bissinger N C. Design and testing of a 2D fixed geometry hypersonic intake. AIAA Paper 98-1529, 1998.
[17]. Walther R, Koschel W, Sabelnikov V, Korontsvit Y, Ivanov V. Investigations into the aerothermodynamic characteristics of scramjet components, International Society for Air Breathing Engines. ISABE Paper 97-7085, 1997.
[18]. Shih T H, Liou W W, Shabbir A, Yang Z and Zhu J. A new κ-ε eddy-viscosity model for high Reynolds number turbulence flows. Computers & Fluids, 1995, 24(3), 227-238.
[19]. Huang W, Wang Z G, Ingham D B, Ma, L and Pourkashanian M. Design exploration for a single expansion ramp nozzle (SERN) using data mining. Acta Astronautica, 2013, 83: 10-17.
[20]. Ding F, Shen C B, Huang W, Liu J. Numerical validation and back-pressure effect on internal compression flows of typical supersonic inlet. The Aeronautical Journal, 2015, 119: 631-645.
[21]. Huang W. Integrated design of interior and exterior flow hypersonic vehicle of near-space and its flight performance. Hunan: National University of Defense Technology, China, 2010.
[22]. Xu X, et al. Stamping engine principle and technology. Beijing: Beijing University of Aeronautics and Astronautics Press, 2014: 104-105.
[23]. Hu K, Li Z B. ANSYS ICEM CFD detailed project examples. Beijing: People Post Press, 2016: 38-40.
[24]. Fluent Inc, ANSYS, Inc, ANSYS FLUENT 15.0 Theory Guide, 2017.
[25]. Launder B E, and Spalding D B. Lectures in mathematical models of turbulence. London: Academic Press, 1972.
[26]. Li P F, Xu M Y, Wang F F. Proficient in CFD engineering simulation and case actual combat. Beijing: People Post Press, 2014: 4-10.
[27]. Li H L. Inlet and structure simulation of a solid - typed Engine. Inner Mongolia: Inner Mongolia University of Technology, 2007.